



OPEN

Programming nonreciprocity and harmonic beam steering via a digitally space-time-coded metamaterial antenna

Shaghayegh Vosoughitabar & Chung-Tse Michael Wu

Recent advancement in digital coding metasurfaces incorporating spatial and temporal modulation has enabled simultaneous control of electromagnetic (EM) waves in both space and frequency domains by manipulating incident EM waves in a transmissive or reflective fashion, resulting in time-reversal asymmetry. Here we show in theory and experiment that a digitally space-time-coded metamaterial (MTM) antenna with spatiotemporal modulation at its unit cell level can be regarded as a radiating counterpart of such digital metasurface, which will enable nonreciprocal EM wave transmission and reception via surface-to-leaky-wave transformation and harmonic frequency generation. Operating in the fast wave (radiation) region, the space-time-coded MTM antenna is tailored in a way such that the propagation constant of each programmable unit cell embedded with varactor diodes can toggle between positive and negative phases, which is done through providing digital sequences by using a field-programmable gate array (FPGA). Owing to the time-varying coding sequence, harmonic frequencies are generated with different main beam directions. Furthermore, the space time modulation of the digitally coded MTM antenna allows for nonreciprocal transmission and reception of EM waves by breaking the time-reversal symmetry, which may enable many applications, such as simultaneous transmitting and receiving, unidirectional transmission, radar sensing, and multiple-input and multiple-output (MIMO) beamformer.

Owing to the fact that the magnetic or electric properties can be modulated periodically in both spatial and temporal domain¹, several space-time modulated architectures have been proposed that can work as a mixer, circulator, transceiver, or nonreciprocal components^{1–11}. Very recently, digitally-coded metasurfaces have appeared to be an effective device to control electromagnetic (EM) waves through manipulating the reflection or transmission phase of each programmable unit cell by switching the integrated PIN diode between on “1” and off “0” states^{12–14}. By changing coding sequences periodically in the time domain, a space-time coding digital metasurface can be realized to provide interesting applications^{15–27}. For example, digitally coded space-time modulation is leveraged to control the pattern of the reflected harmonic waves from the metasurface¹⁵, break the time reversal symmetry by properly designing the digital coding sequences, thereby enabling nonreciprocal wave reflection and frequency conversion¹⁶. In a separate study, a dual-channel wireless communication system utilizing a space-time coding digital metasurface is proposed²⁸. Furthermore, in a recently published research²⁹, a space-time-coding waveguide-integrated metasurface antenna that can control the harmonic patterns independently is realized.

On the other hand, several reconfigurable antennas employing digitally-coded radiating elements have been reported to enable various functionalities. For example, two planar antenna arrays employing digitally coded radiating elements are proposed to control the radiation beams of the antenna in two dimensional space by designing different coding patterns^{30,31}. Furthermore, time modulation has also been applied to the antenna arrays³², in which a predetermined periodic sequence can achieve side lobe reduction for the fundamental frequency pattern³³. Moreover, generated harmonic components can be leveraged to provide physical layer security in wireless communication as well as enable radar detection.^{34–45} Nevertheless, for conventional time modulated antenna arrays, PIN diodes are usually employed as RF switches that decrease the power efficiency due to the power dissipation in their off state⁴⁶.

Recently, not only metasurfaces⁴⁷ but also metamaterial antennas have demonstrated their potential for utilization in wireless communication applications. These include directional modulation transmitters⁴⁸, multiple-input

Department of Electrical and Computer Engineering, Rutgers, the State University of New Jersey, Piscataway, USA.
email: ctm.wu@rutgers.edu

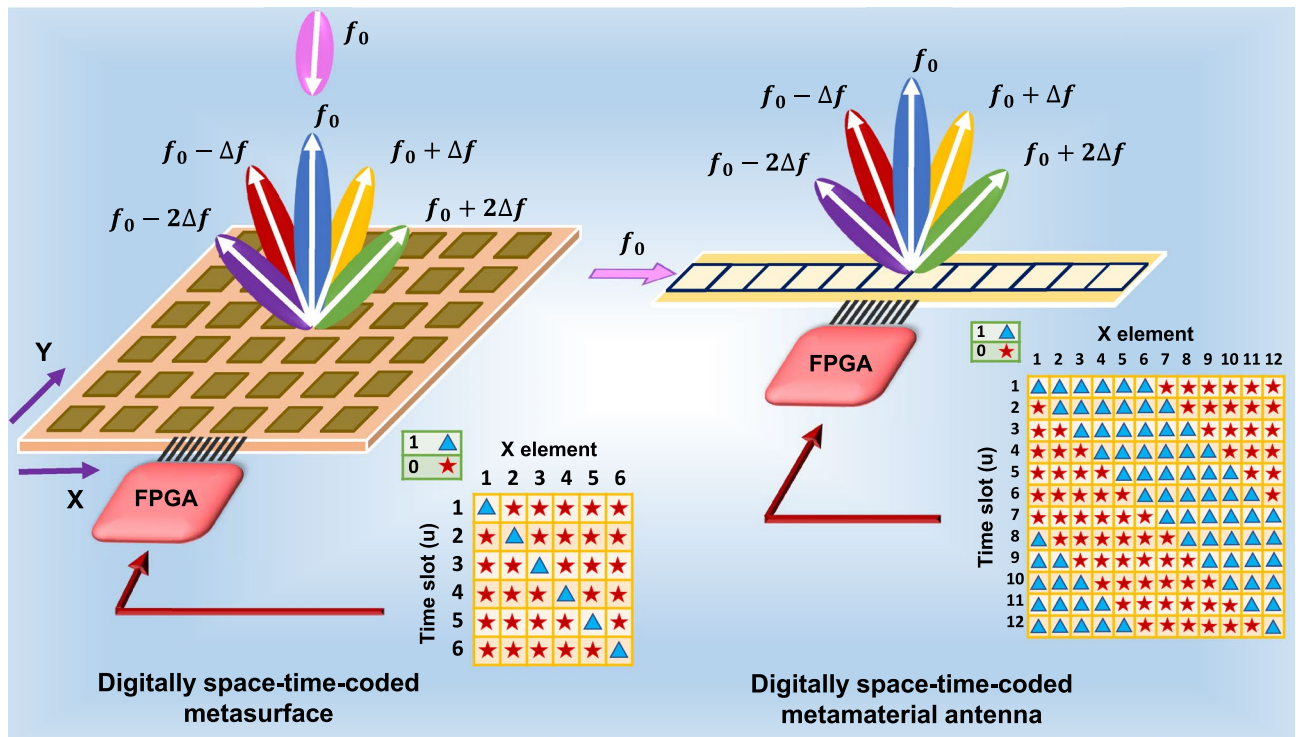


Figure 1. Space-time-modulated metamaterial (ST-MTM) leaky wave antenna as a radiating counterpart of the space-time-modulated metasurface. The space time coding matrices are generated by an FPGA. For the metasurface, the coding sequence is uniform along the Y axis, where “0” and “1” refer to the reflection phase of 0° and 180° , respectively. For the proposed ST-MTM leaky wave antenna, “0” and “1” refer to a negative and positive phase constant (β), respectively.

multiple-output (MIMO) systems⁴⁹, and wireless body area networks⁵⁰, etc. In this work, we propose a programmable space-time digitally modulated composite right/left-handed (CRLH) metamaterial (MTM) leaky wave antenna⁵¹ that can be viewed as a radiating counterpart of the space-time-modulated digital metasurface as shown in Fig. 1. To illustrate, MTMs are artificial EM materials with novel effective medium properties that may not be available in nature. One type of MTM antenna is so-called CRLH transmission line leaky-wave antennas exhibiting continuous backfire-to-endfire frequency-dependent beam scanning with a true broadside main beam. Due to the passive nature, conventional CRLH MTM antennas are reciprocal structures operating at the fundamental dominant mode, which cannot separate transmit and receive signals without an external duplexer. To this end, we show a space-time modulated CRLH MTM antenna with digitally programmable unit cells can enable nonreciprocal EM wave transmission and reception. Moreover, harmonic beam controlling can also be achieved through feeding appropriate coding sequences.

In the case of a space-time-modulated metasurface, an incoming signal at f_0 frequency is illuminated to the surface, whereas the generated harmonics are reflected to the free space. By manipulating the phase and magnitude distribution of the surface through feeding appropriate periodic sequences to each unit cell, harmonic beamforming capability can be achieved. On the other hand, for our proposed space-time metamaterial (ST-MTM) antenna, a signal at f_0 is injected to the antenna input port and the generated harmonics will radiate to the free space. We show theoretically and experimentally that our proposed architecture enables harmonic scanning, simultaneous transmitting and receiving, and nonreciprocal behavior by providing proper spatiotemporal coding sequences for modulating the phase constant of each programmable CRLH MTM unit cell in a periodic fashion. For proof-of-concept realization, varactors are incorporated into each CRLH unit cell to change its phase constant between the positive “state 1” and negative “state 0” values by feeding two specific bias voltages⁵², in which the prespecified periodic sequences are generated by an FPGA and employed as varactors’ control voltages. To the best of the authors’ knowledge, this is the first digitally space-time-coded programmable CRLH MTM antenna exhibiting nonreciprocal and harmonic beamsteering capabilities, which can open up a new paradigm of next-generation intelligent antennas.

Results

Formulation of the radiation pattern of a digitally coded space-time modulated metamaterial (ST-MTM) leaky wave antenna. We first consider a programmable CRLH MTM unit cell consisting of interdigital capacitance and shunt-stub inductance with embedded varactor diodes shown in Supplementary Fig. S1A. The absolute value of phase constant (β) of the designed unit cell multiplied by the unit cell length p versus frequency, known as the dispersion curve, for two different bias voltages of the integrated varactors is

illustrated in Supplementary Fig. S1B. The frequency region under the air line is regarded as the fast wave region in which the CRLH unit cells can radiate. By changing the varactor bias voltage, one can manipulate the dispersion curve of the MTM unit cell, where the phase constant can alternate its polarity under two bias voltages (Bias 1 and Bias 0) at a given frequency located in the fast wave region.

As such, both positive and negative phase constants can be achieved by simply changing the control voltage from Bias 1 to Bias 0, thereby realizing a binary digital MTM radiating unit cell. We denote that state “1” provides positive β and state “0” provides negative β . A leaky wave antenna can thus be achieved by cascading such digital binary CRLH MTM cells, where the input signal operating in fast wave region radiates out as it propagates along the MTM structure. Moreover, by imposing the time modulation, the phase constant of each unit cell, i.e., β , changes with time in a periodic manner. By incorporating the array factor approach⁵³, in the transmit mode, the radiation pattern of a ST-MTM leaky wave antenna with digital coding can be expressed as:

$$R(\theta, t) = S(t) \sum_{n=1}^N e^{-\alpha(n-1)p} e^{jk_q(n-1)p \cos \theta} U_n(t), \tag{1}$$

$$U_n(t) = e^{-j \sum_{m=1}^n \varphi_m(t)} = \sum_{u=1}^L \gamma_n^u H_u(t), \tag{2}$$

$$H_u(t) = \begin{cases} 1 & \frac{(u-1)T}{L} \leq t \leq \frac{uT}{L} \\ 0 & \text{Otherwise,} \end{cases} \tag{3}$$

$$\gamma_n^u = \prod_{m=1}^n e^{-j\varphi_m^u}, \varphi_m^u = \begin{cases} \beta_0 p, & \text{State 0,} \\ \beta_1 p, & \text{State 1,} \end{cases} \text{ in } \frac{(u-1)T}{L} \leq t \leq \frac{uT}{L}, \tag{4}$$

$$H_u(t) = \sum_{q=-\infty}^{\infty} a_{uq} e^{\frac{j2\pi q t}{T}}, \tag{5}$$

where $S(t)$ is the input signal with the frequency f_0 and the magnitude S_0 , which is a sinusoidal wave with frequency f_0 . N is the number of CRLH cells of the leaky wave antenna. p is length of the unit cell, α is leakage factor, and L is length of the sequence in one period ($T = 1/\Delta f$). Moreover, $k_q = 2\pi(f_0 + q\Delta f)/c$ is the propagation constant for the q th radiated harmonic frequency, where c is the light speed. Generated harmonics will radiate into the free space with different propagation constants when modulation frequency (Δf) is not much smaller than the input RF signal frequency (f_0). Each period is divided to L time slots and the phase shift of the signal reaches to the n th unit cell, is a periodic function of time and over the u th time slot is defined as (4). After expansion of $H_u(t)$ in the form of Fourier series shown in (5) and substituting it in (1) and doing some manipulations, finally we obtain (see Supplementary for detailed derivation):

$$R(\theta, t) = \sum_{q=-\infty}^{\infty} e^{-j2\pi t(f_0 - q\Delta f)} \text{sinc}\left(\frac{\pi q}{L}\right) e^{\frac{j\pi q}{L}} \sum_{u=1}^L e^{\frac{-j2\pi q u}{L}} \sum_{n=1}^N \frac{\gamma_n^u}{L} S_0 e^{-\alpha(n-1)p} e^{jk_q(n-1)p \cos \theta}. \tag{6}$$

From (6), it can be seen that the radiated patterns entail both radiation at the fundamental frequency (f_0) and generated harmonic frequencies ($f_0 - q\Delta f$). Therefore, the far-field radiation pattern of the antenna at the q th generated harmonic frequency can be expressed as:

$$R_q^{TX}(\theta) = \text{sinc}\left(\frac{\pi q}{L}\right) e^{\frac{j\pi q}{L}} \sum_{u=1}^L e^{\frac{-j2\pi q u}{L}} \sum_{n=1}^N \frac{\gamma_n^u}{L} S_0 e^{-\alpha(n-1)p} e^{jk_q(n-1)p \cos \theta}. \tag{7}$$

On the other hand, in the receive mode, assuming that the signal at f_0 is illuminated to the digital ST-MTM antenna from the θ angle, and generated harmonics are received from the same port of signal injection in the transmit mode, these patterns can be written as: (see Supplementary for detailed derivation):

$$R_q^{RX}(\theta) = \text{sinc}\left(\frac{\pi q}{L}\right) e^{\frac{j\pi q}{L}} \sum_{u=1}^L e^{\frac{-j2\pi q u}{L}} \sum_{n=1}^N \frac{\gamma_n^u}{L} S_0 e^{-\alpha(n-1)p} e^{jk_0(n-1)p \cos \theta}. \tag{8}$$

The only difference between the Eqs. (8) and (7) is replacing k_q with $k_0 = 2\pi f_0/c$, since the incident signal operates at f_0 in the free space and harmonics are generated when the signal is traveling inside the ST-MTM antenna. The pattern of the harmonic frequencies can be controlled by properly feeding the periodic sequence to each unit cell, thereby enabling several functionalities such as harmonic beam scanning, simultaneous transmitting and receiving, and nonreciprocity. The schematic of the proposed ST-MTM antenna consisting of programmable CRLH unit cells is illustrated in Fig. 2A.

Programmable harmonic beam scanning. As also shown in Fig. 2A, the proposed ST-MTM antenna can exhibit dynamic harmonic beam steering, in which the fundamental and harmonic radiation patterns are plotted in Fig. 2B–D when the signal at the fundamental tone is injected from the left port with $N = L = 12$.

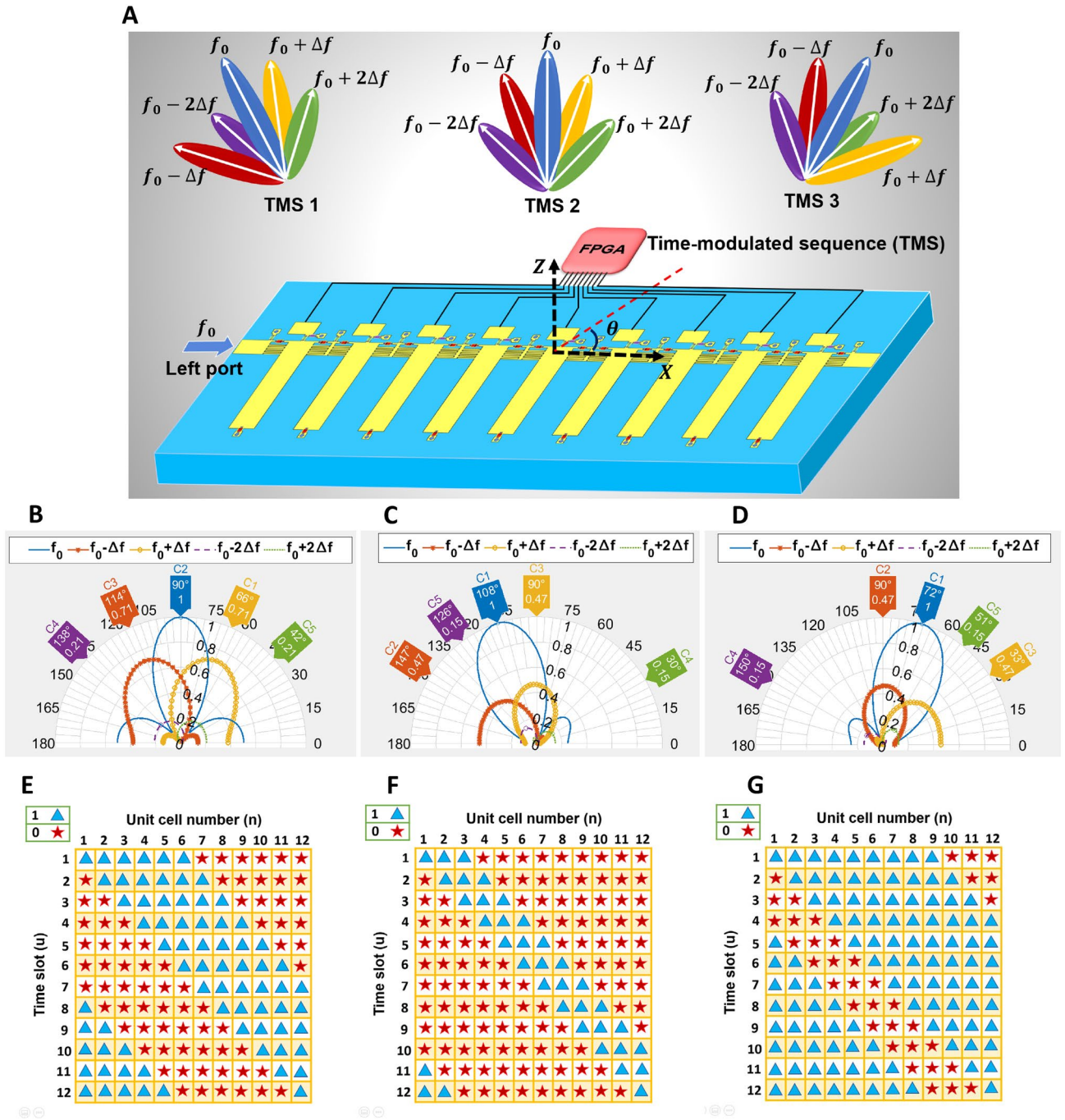


Figure 2. (A) Programmable harmonic beam scanning of the proposed ST-MTM antenna with different space-time coding sequences. Simulated normalized harmonic patterns (dB) when the signal is injected from the left port. (B) for sequence 111110000000. (C) for sequence 111000000000. (D) for sequence 111111110000. State of each unit cell in different time slots in one period for (E) figure (B). (F) figure (C). (G) figure (D).

According to the simulated dispersion diagram of the designed programmable CRLH unit cell in Bias 0 and Bias1 states shown in Supplementary Fig. S1B, the negative and positive phase shift values (β_{0p} , β_{1p}) around 2.05 GHz located in the fast wave are 24 and -24 degrees, respectively. In Fig. 2B the sequence is 111110000000 for the 12 cells in the first time slot and then it is circulated one bit backward for the next time slots as illustrated in Fig. 2E to set the main beam direction of fundamental frequency in broadside. As observed, harmonic beam scanning is achieved by using this sequence, i.e. each harmonic frequency component has its own main beam direction. By changing the sequence to 111000000000 and 111111110000, the main beam of the fundamental frequency and harmonic components can be shifted to the left and right side, respectively, as shown in Fig. 2C,D. Figure 2E,G depict the space time coding matrix corresponding to the patterns shown in Fig. 2C,D (see Supplementary Fig. S4 for more results showing harmonic beam scanning). The resulting harmonic beam scanning

can be utilized in various applications, including multipoint communication purposes or radar sensing systems for multi target detection.

Simultaneous transmitting and receiving. The proposed digitally coded ST-MTM antenna is essentially a 2-port structure and can transmit and receive the information simultaneously as depicted in Fig. 3A. Figure 3B illustrates the case where the fundamental tone signal is injected from the left port, which has the same patterns as Fig. 2B.

Figure 3C illustrates the patterns for injecting the signal from the right port with the same space-time sequence used in Fig. 3B. According to (7) and (8), it can be observed that if $\Delta f \ll f_0$ for each harmonic frequency, the far-field pattern when the signal with f_0 frequency is injected from the left/right port is the same as the received power of that harmonic in different angles from the same port when the signal is illuminated at f_0 frequency to the ST-MTM antenna. Therefore, we can consider Fig. 3C patterns for illuminating the signal at f_0 frequency from different angles and receiving the fundamental signal and harmonic components from the right port. As clearly observed in Fig. 3B,C the patterns are the same for each harmonic frequency when the signal with frequency f_0 is injected from the left and when the signal is illuminated to the ST-MTM antenna, and power levels are recorded from the right port.

Considering this interesting property, the idea of simultaneous transmitting and receiving can be made feasible as illustrated in Fig. 3A. Assuming in the transmit mode, the signal is injected at f_0 frequency from the left port, a transceiver located in the main beam direction of $f_0 + \Delta f$ pattern can receive the signal at $f_0 + \Delta f$ and transmit another signal with this frequency at the same time. In this case under the assumption $\Delta f \ll f_0$, the generated normalized harmonic patterns extracted from the left and right ports are shown in Fig. 3D,E, respectively. According to these figures, $f_0 + \Delta f + \Delta f$, which is the first harmonic in the receive mode, will be the dominant harmonic frequency in this direction and propagates to both right and left ports. As such, the received information can be extracted from the left or right port at $f_0 + 2\Delta f$.

Nonreciprocal behavior of digitally coded ST-MTM antenna. Based on (7) and (8), when the modulation frequency (Δf) is not much smaller than the fundamental frequency (f_0), the main beam direction of harmonic patterns in the transmit mode will be different than their maximum power direction extracted from the same port in the receive mode shown in Fig. 4A. Figure 4B,C illustrate the transmission and reception patterns for different modulation frequencies. According to the results, increasing $\Delta f/f_0$ leads to increasing the difference between the main beam direction of transmission and reception patterns of each harmonic frequency. This property depicts the nonreciprocal behavior of the ST-MTM antenna for $m = \Delta f/f_0 > 0.2$.

Moreover, when f_0 is injected from the left port in transmit mode, consider the main beam direction of generated harmonic pattern with $f_0 + \Delta f$ frequency in $\theta_1 = 66^\circ$ shown in Fig. 3B. In the receive mode under the assumption $\Delta f \ll f_0$, if a signal with $f_0 + \Delta f$ frequency is illuminated to the ST-MTM antenna in different angles, the harmonic patterns extracted from left port are like Fig. 3D by considering $f_0 + \Delta f$ as fundamental frequency. As such, illuminating the signal at $f_0 + \Delta f$ frequency from θ_1 angle to the antenna leads to reception of a very small power at f_0 frequency from the left port, thereby exhibiting nonreciprocal operation.

Experimental verification. As illustrated in Fig. 5A, a prototype of the proposed digitally space-time-coded MTM antenna with 9 unit cells is fabricated to validate the aforementioned concepts. Each unit cell includes three varactors sharing a common bias voltage. According to the dispersion diagram of the unit cell around 2.05 GHz the phase constant can toggle between positive and negative values by changing the bias of varactors from 1 to 0 state. The number of time slots (L) are considered 9 (same as the number of unit cells), and the sequence in the first time slot is shifted by one bit for the next time slot by using an FPGA shown in Fig. 5A. The modulation frequency we apply here is 1.58 MHz, which is much smaller than the fundamental frequency ($\Delta f \ll f_0$). It is worth mentioning that when designing a tunable unit cell with components such as varactors, the switching speed of the varactor should be faster than $L\Delta f$ to ensure effective toggling of β between “0” and “1” states as per the designed time-modulated sequence. Additionally, the capability of the FPGA to generate a periodic signal for driving the varactors, based on its clock frequency, is another factor that may impose limitations on the achievable modulation frequency.

Measured S-parameters of the sample for different time-modulated sequences are plotted in Supplementary Fig. S2, 3, which depict good S_{11} and S_{22} around 2 GHz. In the transmit mode, a signal with a frequency of $f_0 = 2.05$ GHz is injected from the left port of the ST-MTM antenna, and a reference antenna located in the far-field region of the ST-MTM antenna receives the fundamental and harmonic frequencies in different angles. Fig. 5B,C show the normalized measured radiation patterns for sequence 111110000 when the signal is injected from the left and right port, respectively. Based on the aforementioned results shown in Fig. 3, it is expected the main beam directions of fundamental and harmonic frequencies for both left- and right-port excitation should be the same, as can be observed in Fig. 5B,C. To verify the harmonic beam scanning, in Fig. 5D we change the sequence to 110000000, whereas in Fig. 5E the sequence is 111111100, with the signal injected from the left port. As can be seen clearly, with different sequences, the main beam directions of the fundamental and harmonic tones can be steered.

Moreover, Fig. 5F,G depict the measured patterns in the receive mode with the sequence 111110000, when the signal with a frequency of f_0 is illuminated from a reference horn antenna to the ST-MTM antenna at different angles, in which the received spectral components are collected from the left and right port, respectively. The received signals are then normalized to the maximum of the fundamental frequency. It is also expected that the harmonic patterns for the transmit mode and receive mode should be the same, when excited at f_0 , under the condition $\Delta f \ll f_0$, which can be clearly verified from the measured patterns. Furthermore, we then change

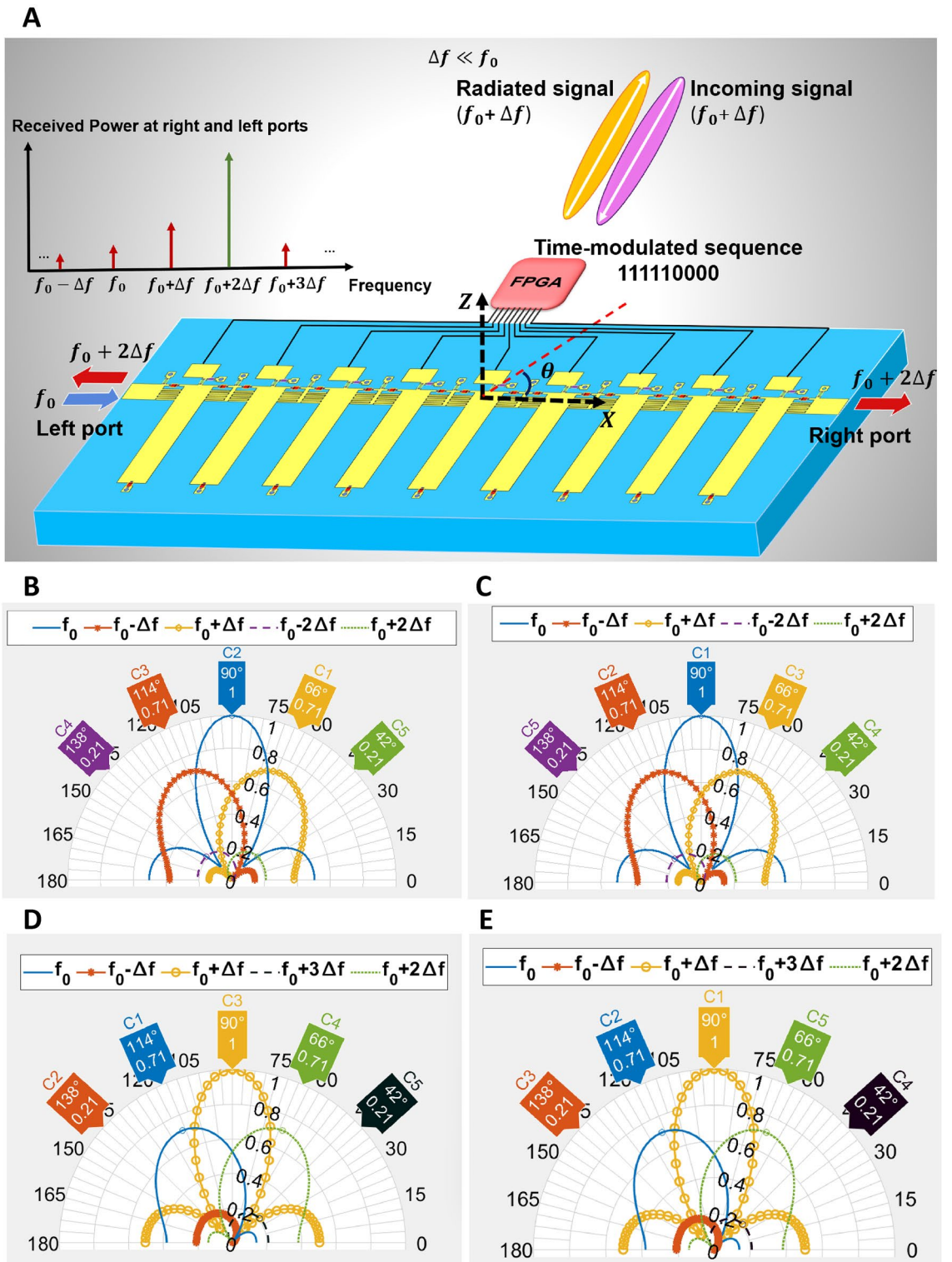


Figure 3. (A) Simultaneous transmitting and receiving by ST-MTM antenna when ($\Delta f \ll f_0$). Simulated normalized harmonic patterns (dB) for sequence 11111000000. (B) when the signal is injected from the left port at f_0 . (C) when the signal is injected from the right port at f_0 . (D) when the signal is illuminated at $f_0 + \Delta f$ and harmonics are received from the left port. (E) when the signal is illuminated at $f_0 + \Delta f$ and harmonics are received from the right port.

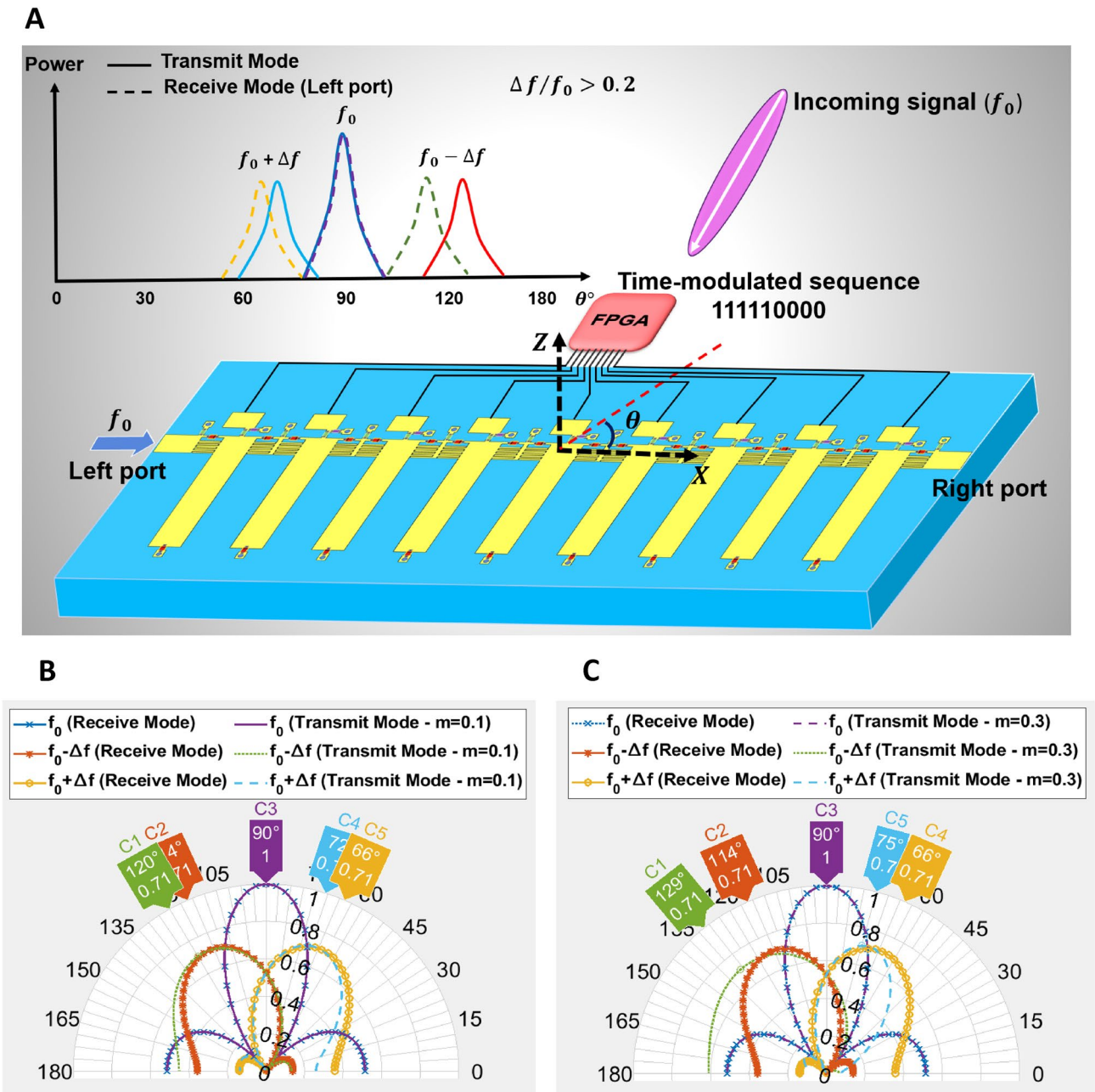


Figure 4. (A) Nonreciprocal behavior for transmission and reception of the signal at harmonic frequencies when $\Delta f/f_0 > 0.2$. Simulated normalized harmonic patterns in transmit mode and receive mode (dB). (B) for $\Delta f/f_0 = 0.1$. (C) for $\Delta f/f_0 = 0.3$.

the illuminated signal frequency to $2.05 \text{ GHz} + \Delta f$, where Δf is 1.58 MHz. The received patterns from the right port are shown in Fig. 5H, where it can be seen that the main beam of $2.05 \text{ GHz} + \Delta f$ is now at the broadside.

It is noticed that the simulated results are based on the antenna with 12 unit cells. Nevertheless, due to the fabrication limitations, we demonstrate a ST-MTM antenna with 9 cells instead. A larger number of MTM unit cells will result in increasing the directivity of the antenna with narrower main beams as can be observed in Fig. 2. While the simulation and measurement results agree with each other, there are some discrepancies in the main beam direction of the fundamental and harmonic frequency patterns, mainly resulting from the difference in unit cell numbers as well as the propagation constant values of the two bias states between the measurement and the full-wave EM simulation. It is noted a small change in the bias voltages come from the FPGA may lead to some deviation of the propagation constant in the two states (0 and 1).

According to the measured results shown in Fig. 5, simultaneous transmitting and receiving is possible based on the proposed approach illustrated in Fig. 3A, where $\Delta f \ll f_0$ for our proposed ST-MTM antenna. On the other hand, the modulation frequency cannot be more than 5.5 MHz due to the hardware limitation of FPGA in the measurement, i.e. the cases when $\Delta f/f_0 > 0.1$.

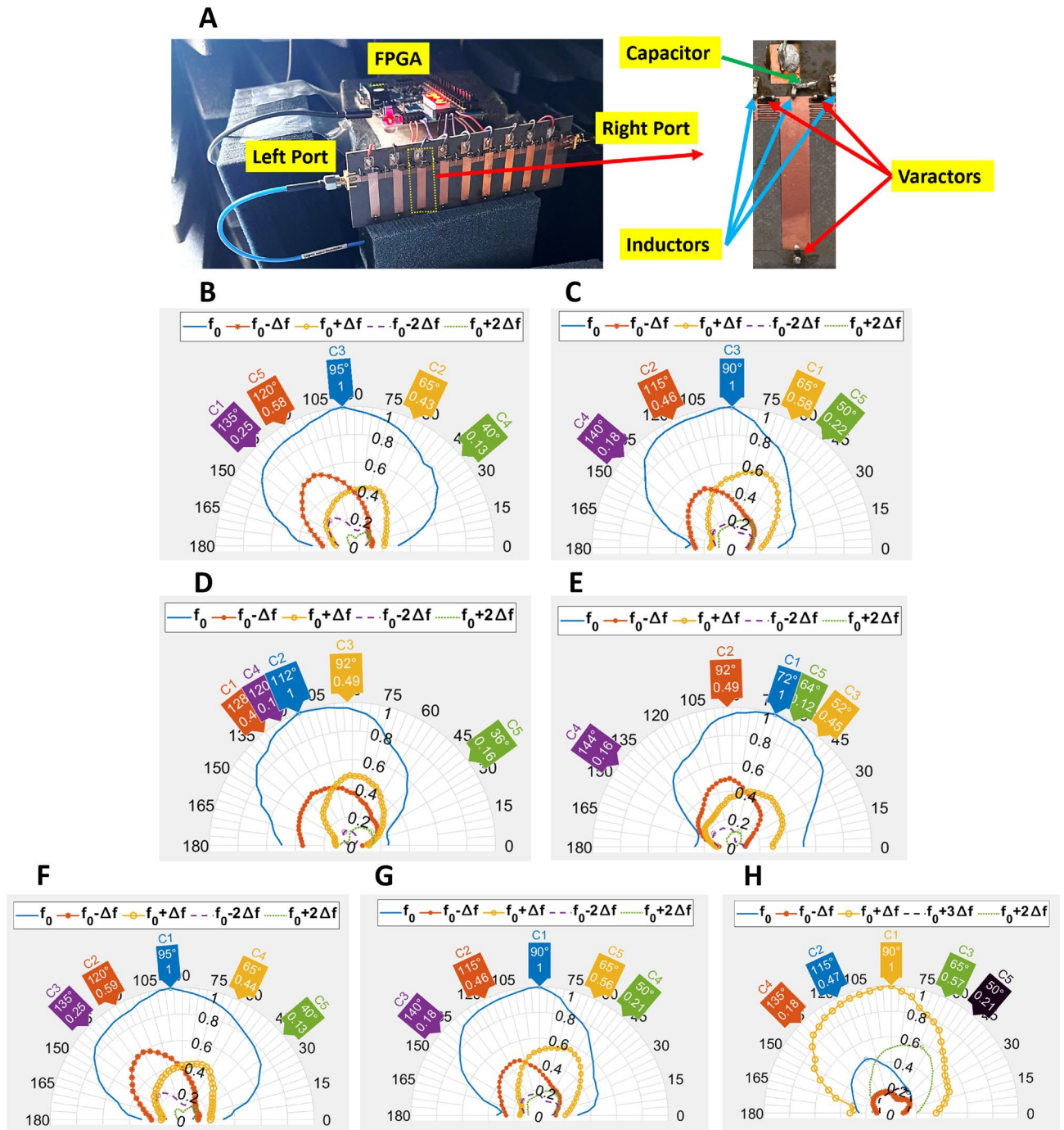


Figure 5. (A) Fabricated prototype of the proposed ST-MTM antenna consisting of 9 programmable CRLH unit cells with the close-up view of the MTM unit cell. (B) Measured normalized harmonic patterns (dB) in the transmit mode with sequence 111110000 when the signal is injected from the left port. (C) The signal is injected from the right port. (D) The signal is injected from the left port with sequence 110000000. (E) sequence 111111100. (F) Receive mode: The ST-MTM antenna is illuminated by a horn antenna at f_0 for sequence 111110000, and signals are received from the left port. (G) from the right port. (H) The ST-MTM antenna is illuminated by a horn antenna at $f_0 + \Delta f$, and the signals are received from the right port for sequence 111110000. In all cases, f_0 is 2.05 GHz and Δf is 1.58 MHz.

Methods

For the theoretical results, MATLAB is used to plot the far field pattern of the fundamental and harmonic frequencies based on the derived equations. For the programmable unit cell design, HFSS as a full wave simulator, is utilized to design the MTM unit cell with dispersion diagrams shown in Supplementary Fig. S1B. The length of the unit cell is around 1.5 cm. In the simulation, the varactors are modeled using a series RLC circuit, where $R = 4.8 \Omega$, $L = 0.7 \text{ nH}$, and C varies with respect to the bias voltages. For the Bias “0” state the capacitor value is

1.05 pF and for Bias “1” state it is 2.1 pF. The prototype is simulated and fabricated on a RO5870 substrate with a dielectric constant of 2.33 and thickness of 1.57 mm. The varactors are SMV2019 from Skyworks, where the capacitance range varies from 2.2 pF at a bias voltage of 0 V to 0.3 pF at 20 V. It is noted 0.1 V and 3 V can provide our design with the required positive and negative phase constants, respectively.

Basys 3 FPGA board is used to provide 9 digital outputs for the control bias voltages of each unit cell. The low-level output voltage is around 50 mV, whereas the high-level one is around 3.2 V, which can provide us the 0 and 1 states for the predetermined sequences. The period of the time coding sequence is selected to be 0.63 μ s, resulting in a modulation frequency of 1.58 MHz. The radiation pattern measurements are conducted inside a microwave anechoic chamber. A reference horn antenna is used as a transmitter when the prototype operates in the receive mode, and as a receiver when the prototype operates as a transmitter. A signal generator is utilized to provide a signal in the frequency of around 2 GHz. By using a spectrum analyzer, the received signals at the fundamental and harmonic frequencies are collected from the reference horn antenna in the transmit mode, as well as from the left and right port of the prototype in the receive mode when illuminated from different angles.

Discussion

In this paper, we propose a digitally space-time-coded MTM antenna exhibiting harmonic beam scanning and nonreciprocity behavior, which can be used for simultaneous transmitting and receiving. The phase constant of each varactor-embedded programmable CRLH unit cell changes between positive (state 1), and negative (state 0) values based on a predetermined sequence in a periodic fashion in both space and time domain. In so doing, harmonic beam scanning can be realized by simply changing the programming coding sequences, which may lead to various applications including MIMO communication and radar detection.

Moreover, nonreciprocal transmission and reception of harmonic waves can be achieved by the proposed ST-MTM antenna. When $\Delta f \ll f_0$, the generated harmonic signal at $f_0 + \Delta f$ will radiate towards a specific direction in the transmit mode, while in the receive mode, by illuminating a signal at $f_0 + \Delta f$ to the ST-MTM antenna at the same direction, the dominant generated harmonic signal becomes $f_0 + 2\Delta f$. Leveraging such nonreciprocal property, simultaneous transmitting and receiving can therefore be realized by transmitting the signal at f_0 , whereas the information of the receiving signal can be extracted at the frequency of $f_0 + 2\Delta f$.

On the other hand, when the modulation frequency is not much smaller than the fundamental frequency, different main beam directions of harmonic waves for transmit and receive patterns can be observed when injecting or illuminating the antenna at the same frequency. A prototype with 9 programmable MTM unit cells is fabricated, in which the experimental results validate the proposed concept of the ST-MTM antenna.

Data availability

The data that support the findings of this study are available from the corresponding author upon reasonable request.

Received: 2 March 2023; Accepted: 25 April 2023

Published online: 05 May 2023

References

1. Taravati, S. & Kishk, A. A. Space-time modulation: Principles and applications. *IEEE Microw. Mag.* **21**, 30–56. <https://doi.org/10.1109/MMM.2019.2963606> (2020).
2. Taravati, S. & Caloz, C. Mixer-duplexer-antenna leaky-wave system based on periodic space-time modulation. *IEEE Trans. Antennas Propag.* **65**, 442–452. <https://doi.org/10.1109/TAP.2016.2632735> (2017).
3. Qin, S., Xu, Q. & Wang, Y. E. Nonreciprocal components with distributedly modulated capacitors. *IEEE Trans. Microw. Theory Tech.* **62**, 2260–2272. <https://doi.org/10.1109/TMTT.2014.2347935> (2014).
4. Hadad, Y., Soric, J. C. & Alu, A. Breaking temporal symmetries for emission and absorption. *Proc. Natl. Acad. Sci.* **113**, 3471–3475. <https://doi.org/10.1073/pnas.1517363113> (2016).
5. Taravati, S. & Eleftheriades, G. V. Microwave space-time-modulated metasurfaces. *ACS Photonics* **9**, 305–318. <https://doi.org/10.1021/acsp Photonics.1c01041> (2022).
6. Estep, N. A., Sounas, D. L. & Alù, A. Magnetless microwave circulators based on spatiotemporally modulated rings of coupled resonators. *IEEE Trans. Microw. Theory Tech.* **64**, 502–518. <https://doi.org/10.1109/TMTT.2015.2511737> (2016).
7. Vosoughitabar, S., Zhu, M. & Wu, C.-T. M. A distributed mixer-based nonreciprocal crlh leaky wave antenna for simultaneous transmit and receive. In *2021 IEEE MTT-S International Microwave Symposium (IMS)*, 408–411. <https://doi.org/10.1109/IMS19712.2021.9574840> (2021).
8. Bukhari, S. S., Vardaxoglou, J. Y. & Whittow, W. A metasurfaces review: Definitions and applications. *Appl. Sci.* <https://doi.org/10.3390/app9132727> (2019).
9. Taravati, S. Aperiodic space-time modulation for pure frequency mixing. *Phys. Rev. B* **97**, 115131. <https://doi.org/10.1103/PhysRevB.97.115131> (2018).
10. Ramaccia, D., Bilotti, F. & Toscano, A. Angular momentum-biased metamaterials for filtering waveguide components and antennas with non-reciprocal behavior. In *2014 8th International Congress on Advanced Electromagnetic Materials in Microwaves and Optics*, 250–252. <https://doi.org/10.1109/MetaMaterials.2014.6948664> (2014).
11. Taravati, S. & Eleftheriades, G. V. Full-duplex nonreciprocal beam steering by time-modulated phase-gradient metasurfaces. *Phys. Rev. Appl.* **14**, 014027. <https://doi.org/10.1103/PhysRevApplied.14.014027> (2020).
12. Bao, L. *et al.* Design of digital coding metasurfaces with independent controls of phase and amplitude responses. *Appl. Phys. Lett.* **113**, 063502. <https://doi.org/10.1063/1.5043520> (2018).
13. Ma, Q. *et al.* Digital coding metasurfaces: From theory to applications. *IEEE Antennas Propag. Mag.* **64**, 96–109. <https://doi.org/10.1109/MAP.2022.3169397> (2022).
14. Ma, Q. *et al.* Controllable and programmable nonreciprocity based on detachable digital coding metasurface. *Adv. Opt. Mater.* **7**, 1901285. <https://doi.org/10.1002/adom.201901285> (2019).
15. Zhang, L. *et al.* Space-time-coding digital metasurfaces. *Nat. Commun.* **9**, 1–11 (2018).
16. Zhang, L. *et al.* Breaking reciprocity with space-time-coding digital metasurfaces. *Adv. Mater.* **31**, 1904069. <https://doi.org/10.1002/adma.201904069> (2019).

17. Dai, J. Y. *et al.* Wireless communication based on information metasurfaces. *IEEE Trans. Microw. Theory Tech.* **69**, 1493–1510. <https://doi.org/10.1109/TMTT.2021.3054662> (2021).
18. Zhang, L., Chen, X. Q., Cheng, Q. & Cui, T. J. Space-time-coding digital metasurfaces for new-architecture wireless communications. In *2022 16th European Conference on Antennas and Propagation (EuCAP)*, 1–4. <https://doi.org/10.23919/EuCAP53622.2022.9769603> (2022).
19. Zhao, J. *et al.* Programmable time-domain digital-coding metasurface for non-linear harmonic manipulation and new wireless communication systems. *Natl. Sci. Rev.* **6**, 231–238. <https://doi.org/10.1093/nsr/nwy135> (2018).
20. Dai, J. Y. *et al.* Realization of multi-modulation schemes for wireless communication by time-domain digital coding metasurface. *IEEE Trans. Antennas Propag.* **68**, 1618–1627. <https://doi.org/10.1109/TAP.2019.2952460> (2020).
21. Dai, J. Y. *et al.* Wireless communications through a simplified architecture based on time-domain digital coding metasurface. *Adv. Mater. Technol.* **4**, 1900044. <https://doi.org/10.1002/admt.201900044> (2019).
22. Li, L., Zhao, H., Liu, C., Li, L. & Cui, T. J. Intelligent metasurfaces: Control, communication and computing. *eLight*. <https://doi.org/10.1186/s43593-022-00013-3> (2022).
23. Wu, H. *et al.* Harmonic information transitions of spatiotemporal metasurfaces. *Light Sci. Appl.* <https://doi.org/10.1038/s41377-020-00441-1> (2020).
24. Dai, J. Y. *et al.* High-efficiency synthesizer for spatial waves based on space-time-coding digital metasurface. *Laser Photonics Rev.* **14**, 1900133. <https://doi.org/10.1002/lpor.201900133> (2020).
25. Zhang, L. & Cui, T. J. Space-time-coding digital metasurfaces: Principles and applications. *Research* **2021**, 1–25. <https://doi.org/10.34133/2021/9802673> (2021).
26. Liu, B., Wong, S.-W. & Li, Y. Rotational doppler effect by space-time-coding metasurfaces for nonreciprocal electromagnetic isolation. *Opt. Express* **29**, 24500–24507. <https://doi.org/10.1364/OE.432886> (2021).
27. Cui, T. J., Qi, M. Q., Wan, X., Zhao, J. & Cheng, Q. Coding metamaterials, digital metamaterials and programmable metamaterials. *Light Sci. Appl.* **3**, e218–e218. <https://doi.org/10.1038/lsa.2014.99> (2014).
28. Zhang, L. *et al.* A wireless communication scheme based on space- and frequency-division multiplexing using digital metasurfaces. *Nat. Electron.* **4**, 218–227. <https://doi.org/10.1038/s41928-021-00554-4> (2021).
29. Wu, G.-B., Dai, J. Y., Cheng, Q., Cui, T. J. & Chan, C. H. Sideband-free space-time-coding metasurface antennas. *Nat. Electron.* **5**, 808–819. <https://doi.org/10.1038/s41928-022-00857-0> (2022).
30. Zhang, X. G., Jiang, W. X., Tian, H. W. & Cui, T. J. Controlling radiation beams by low-profile planar antenna arrays with coding elements. *ACS Omega* **3**, 10601–10611. <https://doi.org/10.1021/acsomega.8b01679> (2018) (PMID: 31459183).
31. Zhang, X. G. *et al.* Pattern-reconfigurable planar array antenna characterized by digital coding method. *IEEE Trans. Antennas Propag.* **68**, 1170–1175. <https://doi.org/10.1109/TAP.2019.2938678> (2020).
32. Maneiro-Catoira, R., Brégains, J., Garcia-Naya, J. A. & Castedo, L. Time modulated arrays: From their origin to their utilization in wireless communication systems. *Sensors*. <https://doi.org/10.3390/s17030590> (2017).
33. Yan, K.-K. & Lu, Y. Sidelobe reduction in array-pattern synthesis using genetic algorithm. *IEEE Trans. Antennas Propag.* **45**, 1117–1122. <https://doi.org/10.1109/8.596902> (1997).
34. He, C., Wang, L., Chen, J. & Jin, R. Time-modulated arrays: A four-dimensional antenna array controlled by switches. *J. Commun. Inf. Netw.* **3**, 1–14. <https://doi.org/10.1007/s41650-018-0004-7> (2018).
35. Shan, C., Ma, Y., Zhao, H. & Shi, J. Joint radar-communications design based on time modulated array. *Digit. Signal Process.* **82**, 43–53. <https://doi.org/10.1016/j.dsp.2018.07.013> (2018).
36. Euzière, J., Guinvarc’h, R., Uguen, B. & Gillard, R. Optimization of sparse time-modulated array by genetic algorithm for radar applications. *IEEE Antennas Wirel. Propag. Lett.* **13**, 161–164. <https://doi.org/10.1109/LAWP.2014.2299285> (2014).
37. Poli, L., Rocca, P., Oliveri, G. & Massa, A. Harmonic beamforming in time-modulated linear arrays. *IEEE Trans. Antennas Propag.* **59**, 2538–2545. <https://doi.org/10.1109/TAP.2011.2152323> (2011).
38. Zhu, Q., Yang, S., Yao, R. & Nie, Z. Directional modulation based on 4-D antenna arrays. *IEEE Trans. Antennas Propag.* **62**, 621–628. <https://doi.org/10.1109/TAP.2013.2290122> (2014).
39. Li, H., Chen, Y. & Yang, S. Directional modulation in time-modulated array with a novel pseudorandom ascending phase time sequence. *IEEE Trans. Microw. Theory Tech.* **70**, 3319–3328. <https://doi.org/10.1109/TMTT.2022.3167693> (2022).
40. Rezaei Aghdam, S., Nooraiepour, A. & Duman, T. M. An overview of physical layer security with finite-alphabet signaling. *IEEE Commun. Surv. Tutor.* **21**, 1829–1850. <https://doi.org/10.1109/COMST.2018.2880421> (2019).
41. Nusenu, S. Y., Huaizong, S., Pan, Y. & Basit, A. Directional modulation with precise legitimate location using time-modulation retrodirective frequency diversity array for secure IoT communications. *IEEE Syst. J.* **15**, 1109–1119. <https://doi.org/10.1109/JSYST.2020.3010787> (2021).
42. Nooraiepour, A., Vosoughitabar, S., Wu, C.-T.M., Bajwa, W. U. & Mandayam, N. B. Time-varying metamaterial-enabled directional modulation schemes for physical layer security in wireless communication links. *J. Emerg. Technol. Comput. Syst.* <https://doi.org/10.1145/3513088> (2022).
43. Tennant, A. & Chambers, B. A two-element time-modulated array with direction-finding properties. *IEEE Antennas Wirel. Propag. Lett.* **6**, 64–65. <https://doi.org/10.1109/LAWP.2007.891953> (2007).
44. Kanbaz, I., Yesilyurt, U. & Aksoy, E. Range-angle dependent radiation by using non-uniform period time modulated arrays. In *2021 IEEE Microwave Theory and Techniques in Wireless Communications (MTTW)*, 223–227. <https://doi.org/10.1109/MTTW53539.2021.9607243> (2021).
45. Li, G., Yang, S. & Nie, Z. Direction of arrival estimation in time modulated linear arrays with unidirectional phase center motion. *IEEE Trans. Antennas Propag.* **58**, 1105–1111. <https://doi.org/10.1109/TAP.2010.2041313> (2010).
46. Yang, S., Gan, Y. B. & Tan, P. K. Evaluation of directivity and gain for time-modulated linear antenna arrays. *Microw. Opt. Technol. Lett.* **42**, 167–171. <https://doi.org/10.1002/mop.20241> (2004).
47. Zhang, X. G. *et al.* A metasurface-based light-to-microwave transmitter for hybrid wireless communications. *Light Sci. Appl.* **11**, 126. <https://doi.org/10.1038/s41377-022-00817-5> (2022).
48. Vosoughitabar, S., Nooraiepour, A., Bajwa, W. U., Mandayam, N. & Wu, C.-T. M. Metamaterial-enabled 2D directional modulation array transmitter for physical layer security in wireless communication links. In *2022 IEEE/MTT-S International Microwave Symposium—IMS 2022*, 595–598. <https://doi.org/10.1109/IMS37962.2022.9865545> (2022).
49. Kumar, S. & Singh, H. A comprehensive review of metamaterials/metasurface-based MIMO antenna array for 5G millimeter-wave applications. *J. Supercond. Novel Magn.* **35**, 3025–3049. <https://doi.org/10.1007/s10948-022-06408-0> (2022).
50. Zhang, K., Soh, P. J. & Yan, S. Meta-wearable antennas—A review of metamaterial based antennas in wireless body area networks. *Materials*. <https://doi.org/10.3390/ma14010149> (2021).
51. Itoh, T. & Caloz, C. *Electromagnetic Metamaterials: Transmission Line Theory and Microwave Applications* (Wiley, 2005).
52. Lim, S., Caloz, C. & Itoh, T. Metamaterial-based electronically controlled transmission-line structure as a novel leaky-wave antenna with tunable radiation angle and beamwidth. *IEEE Trans. Microw. Theory Tech.* **53**, 161–173. <https://doi.org/10.1109/TMTT.2004.839927> (2005).
53. Luo, Y. *et al.* Active metamaterial antenna with beam scanning manipulation based on a digitally modulated array factor method. *IEEE Trans. Antennas Propag.* **69**, 1198–1203. <https://doi.org/10.1109/TAP.2020.3010941> (2021).

Acknowledgements

This work was supported by the National Science Foundation (NSF) under Grant ECCS-2229384 and ECCS-2028823. Any opinions, findings, and conclusions or recommendations expressed in this material are those of the authors and do not necessarily reflect the views of the National Science Foundation.

Author contributions

Conceptualization: C.-T.M.W.; design, prototyping, experiments and data collection: S.V.; Writing—original draft: S.V.; writing—review & editing: C.-T.M.W.

Competing interests

The authors declare no competing interests.

Additional information

Supplementary Information The online version contains supplementary material available at <https://doi.org/10.1038/s41598-023-34195-8>.

Correspondence and requests for materials should be addressed to C.-T.M.W.

Reprints and permissions information is available at www.nature.com/reprints.

Publisher's note Springer Nature remains neutral with regard to jurisdictional claims in published maps and institutional affiliations.



Open Access This article is licensed under a Creative Commons Attribution 4.0 International License, which permits use, sharing, adaptation, distribution and reproduction in any medium or format, as long as you give appropriate credit to the original author(s) and the source, provide a link to the Creative Commons licence, and indicate if changes were made. The images or other third party material in this article are included in the article's Creative Commons licence, unless indicated otherwise in a credit line to the material. If material is not included in the article's Creative Commons licence and your intended use is not permitted by statutory regulation or exceeds the permitted use, you will need to obtain permission directly from the copyright holder. To view a copy of this licence, visit <http://creativecommons.org/licenses/by/4.0/>.

© The Author(s) 2023